JCI The Journal of Clinical Investigation

HGF-MET signals via the MLL-ETS2 complex in hepatocellular carcinoma

Shugaku Takeda, … , Emily H. Cheng, James J. Hsieh

J Clin Invest. 2013;123(7):3154-3165. https://doi.org/10.1172/JCI65566.

Research Article

HGF signals through its cognate receptor, MET, to orchestrate diverse biological processes, including cell proliferation, cell fate specification, organogenesis, and epithelial-mesenchymal transition. Mixed-lineage leukemia (MLL), an epigenetic regulator, plays critical roles in cell fate, stem cell, and cell cycle decisions. Here, we describe a role for MLL in the HGF-MET signaling pathway. We found a shared phenotype among *Mll*$^{-/-}$, *Hgf*$^{-/-}$, and *Met*$^{-/-}$ mice with common cranial nerve XII (CNXII) outgrowth and myoblast migration defects. Phenotypic analysis demonstrated that MLL was required for HGF-induced invasion and metastatic growth of hepatocellular carcinoma cell lines. HGF-MET signaling resulted in the accumulation of ETS2, which interacted with MLL to transactivate MMP1 and MMP3. ChIP assays demonstrated that activation of the HGF-MET pathway resulted in increased occupancy of the MLL-ETS2 complex on *MMP1* and *MMP3* promoters, where MLL trimethylated histone H3 lysine 4 (H3K4), activating transcription. Our results present an epigenetic link between MLL and the HGF-MET signaling pathway, which may suggest new strategies for therapeutic intervention.

Find the latest version:

https://jci.me/65566/pdf

 Related Commentary, page 2780

HGF-MET signals via the MLL-ETS2 complex in hepatocellular carcinoma

Shugaku Takeda,[1] Han Liu,[1] Satoru Sasagawa,[2] Yiyu Dong,[1] Paul A. Trainor,[3,4] Emily H. Cheng,[1,5] and James J. Hsieh[1,6,7]

[1]Human Oncology and Pathogenesis Program, Memorial Sloan-Kettering Cancer Center, New York, New York, USA. [2]Department of Biology, Osaka Medical Center for Cancer and Cardiovascular Diseases, Osaka, Japan. [3]Stowers Institute for Medical Research, Kansas City, Missouri, USA. [4]Department of Anatomy and Cell Biology, University of Kansas Medical Center, Kansas City, Kansas, USA. [5]Department of Pathology and [6]Department of Medicine, Memorial Sloan-Kettering Cancer Center, New York, New York, USA. [7]Department of Medicine, Weill Medical College of Cornell University, New York, New York, USA.

HGF signals through its cognate receptor, MET, to orchestrate diverse biological processes, including cell proliferation, cell fate specification, organogenesis, and epithelial-mesenchymal transition. Mixed-lineage leukemia (MLL), an epigenetic regulator, plays critical roles in cell fate, stem cell, and cell cycle decisions. Here, we describe a role for MLL in the HGF-MET signaling pathway. We found a shared phenotype among *Mll*$^{-/-}$, *Hgf*$^{-/-}$, and *Met*$^{-/-}$ mice with common cranial nerve XII (CNXII) outgrowth and myoblast migration defects. Phenotypic analysis demonstrated that MLL was required for HGF-induced invasion and metastatic growth of hepatocellular carcinoma cell lines. HGF-MET signaling resulted in the accumulation of ETS2, which interacted with MLL to transactivate MMP1 and MMP3. ChIP assays demonstrated that activation of the HGF-MET pathway resulted in increased occupancy of the MLL-ETS2 complex on *MMP1* and *MMP3* promoters, where MLL trimethylated histone H3 lysine 4 (H3K4), activating transcription. Our results present an epigenetic link between MLL and the HGF-MET signaling pathway, which may suggest new strategies for therapeutic intervention.

Introduction

Binding of individual growth factors to their respective receptor tyrosine kinases (RTKs) initiates signaling cascades that coordinate key cellular processes, such as proliferation, differentiation, survival, death, migration, and invasion (1). Hence, their activity needs to be tightly controlled, and aberrations commonly contribute to the pathogenesis of human cancers. *HGF* (also known as scatter factor; *SF*) encodes a highly versatile growth factor that was initially discovered based on activity in dispersing Madin-Darby canine kidney (MDCK) cells and promotion of hepatocyte proliferation (2, 3). The cognate cell surface receptor for HGF was subsequently demonstrated to be the proto-oncogene MET, which regulates cell fate, tissue growth, organogenesis, and neurite outgrowth (4). The HGF-MET signaling cascade channels through a myriad of intermediate signal transduction molecules to transcription factors, which ultimately activates expression of effectors that execute the respective cellular processes. Furthermore, excessive HGF-MET signals render invasive and metastatic phenotypes of affected human cancers (4). Although upstream signaling events and several key downstream effectors of the HGF-MET pathway have been characterized, the signaling relay from the plasma membrane–bound MET to DNA sequence–specific transcription factors remains unclear.

Regulated extracellular proteolysis is essential in maintaining tissue homeostasis. In cancer, deregulated extracellular proteolysis, which is mainly mediated by MMPs, contributes to the tumor invasion and metastasis phenotype (5, 6). At steady state, most tissues express low levels of MMPs, which can be induced and activated by inflammatory cytokines, hormones, growth factors, and cellular transformation. HGF is known to upregulate MMP1, MMP3, MMP7, and MMP9 in a range of epithelial and carcinoma cells, strongly correlating with induced invasiveness (7–11). Interestingly, shared regulatory DNA elements have been identified in the promoters of these inducible MMPs, including binding sites for E-twenty six (ETS) transcription factors, which are required for Ras-induced overexpression of the respective MMPs (12–14).

The mixed-lineage leukemia (*MLL*) gene, a human analog of *trithorax* in *Drosophila*, encodes an epigenetic transcriptional regulator belonging to the trithorax group family. The best-known developmental role of MLL is to maintain proper expression of Hox genes and thus orchestrate the segmental body plan (15–17). Consequently, mice deficient for *Mll* (*Mll*$^{+/-}$ and *Mll*$^{-/-}$) display homeotic transformation (18). In addition to patterning axial skeletons, MLL also regulates hematopoiesis and cell cycle (18–21). MLL possesses histone H3 lysine 4–specific (H3K4-specific) histone methyl transferase (HMT) activity (17, 22–25). H3K4 trimethylation (H3K4me3) catalyzed by MLL activates transcription, leading to orchestrated upregulation of key developmental genes, such as Hox genes (23, 24, 26, 27). Notably, the activity of MLL is modulated by posttranslational modifications, such as phosphorylation, ubiquitination, and proteolysis (20, 21, 28, 29). MLL undergoes site-specific proteolytic cleavage by taspase-1 (encoded by *TASP1*), which gives rise to a mature 500-kDa MLL$^{N320/C180}$ heterodimer (28). In the absence of taspase-1, MLL exists as a noncleaved precursor with reduced HMT activity. Hence, taspase-1–mediated MLL proteolysis is required to generate a fully functional MLL (26). Subsequent studies identified additional bona fide taspase-1 substrates, including MLL2 (also known as MLL4), TFIIA, TFIIA-like factor (ALF), and host cell factor 1 (HCF-1) (26, 30, 31).

To investigate what biological processes are controlled by taspase-1–mediated MLL proteolysis, we created *Mll*$^{nc/nc}$ mice, in

Conflict of interest: The authors have declared that no conflict of interest exists.
Citation for this article: *J Clin Invest.* 2013;123(7):3154–3165. doi:10.1172/JCI65566.

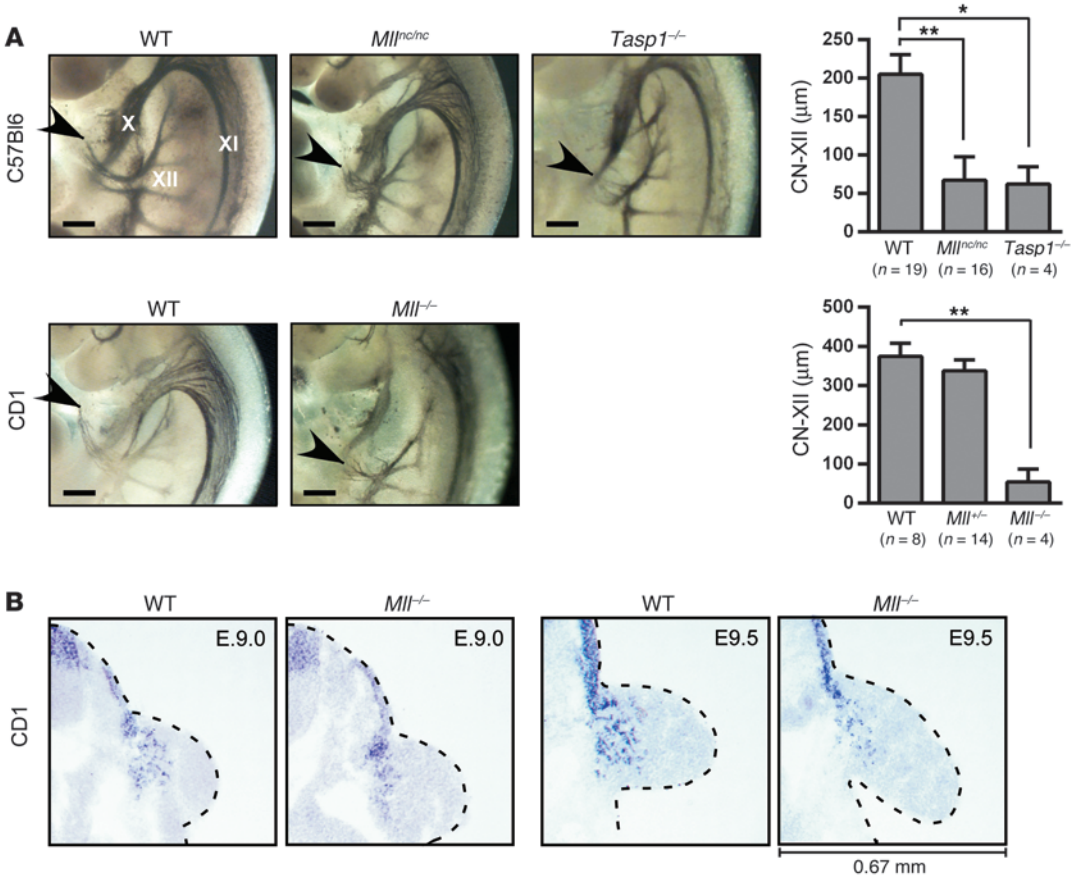

Figure 1

Mll$^{-/-}$ mice exhibit CNXII outgrowth and myoblast migration defects. (**A**) Lateral views of E10.5 embryos (somite #36) stained with the 2H3 anti-neurofilament Ab to visualize CNXII of WT, *Mll*$^{nc/nc}$, and *Tasp1*$^{-/-}$ embryos (C57BL/6 background) or WT and *Mll*$^{-/-}$ embryos (CD1 background). Distance from the crossover of CNXII and CNX to the distal end of CNXII (arrowhead) was quantified and presented as mean ± SEM. *P < 0.05; **P < 0.01. Scale bars: 0.2 mm. (**B**) In situ hybridization on sections of E9.0 (somite #24) and E9.5 (somite #27) WT and *Mll*$^{-/-}$ embryos using a specific RNA probe against *Pax3* mRNA was performed to visualize migratory myoblasts. Representative images of dermomyotomes at forelimbs are shown. Dashed outlines denote the exterior surface of the embryos at the forelimb bud level.

which noncleavable (nc) mutations were engineered into the endogenous *Mll* locus. As expected, *Mll*$^{nc/nc}$ mice exhibited homeotic defects consistent with the role of taspase-1–mediated MLL proteolysis in regulating Hox gene expression. Unexpectedly, these embryos also displayed impaired outgrowth of cranial nerve XII (CNXII; also known as the hypoglossal nerve), a process regulated by the HGF-MET signaling pathway, but not by Hox genes (32, 33). Genetic study of *Tasp1*$^{-/-}$ and *Mll*$^{-/-}$ embryos identified the same CNXII outgrowth defect, indicating the requirement of a fully functional MLL for the proper outgrowth of CNXII. Furthermore, defects in myoblast migration, another process controlled by the HGF-MET pathway, were also observed in *Mll*$^{-/-}$ embryos. These findings suggested that MLL plays an integral role in the HGF-MET signaling pathway, which was further supported by our ex vivo experiments demonstrating that hindbrain explants from *Mll*$^{-/-}$ embryos were defective in neurite outgrowth toward HGF. Furthermore, both in vitro and in vivo studies indicated that HGF-induced invasion of the hepatocellular carcinoma cell lines HepG2 and HLE required MLL. Molecularly, upon activation of the HGF-MET signaling pathway, an MLL-ETS2 complex was stabilized, which activated the transcription of downstream effectors *MMP1* and *MMP3* to execute the cellular invasion phenotype. Together, our novel findings suggest Hox-independent engagement of MLL in the HGF-MET signaling pathway, elucidate downstream molecular details by which HGF-MET potentiates cellular invasion, and present a signaling cascade originated from a cell surface–anchored receptor through transcription complexes to extracellular matrix remodeling enzymes.

Results

Mll$^{nc/nc}$ *mice exhibit classical homeotic developmental defects.* To investigate how taspase-1–mediated MLL proteolysis regulates biological pathways in vivo, we generated *Mll*$^{nc/nc}$ mice, which carry homozygous noncleavable alleles of *Mll* in which the genomic sequences corresponding to the taspase-1 recognition D/GX motif of cleavage sites 1 and 2 were replaced with A/AA (Supplemental Figure 1A; supplemental material available online with this article; doi:10.1172/JCI65566DS1). Western blots showed that the 500-kDa full-length precursor MLL remained unprocessed in *Mll*$^{nc/nc}$ mouse embryos (Supplemental Figure 1B). *Mll*$^{nc/nc}$ mice were born at the expected Mendelian ratio (*Mll*$^{+/+}$, n = 50; *Mll*$^{nc/+}$, n = 99; *Mll*$^{nc/nc}$, n = 53), but slightly smaller than their WT littermates (Supplemen-

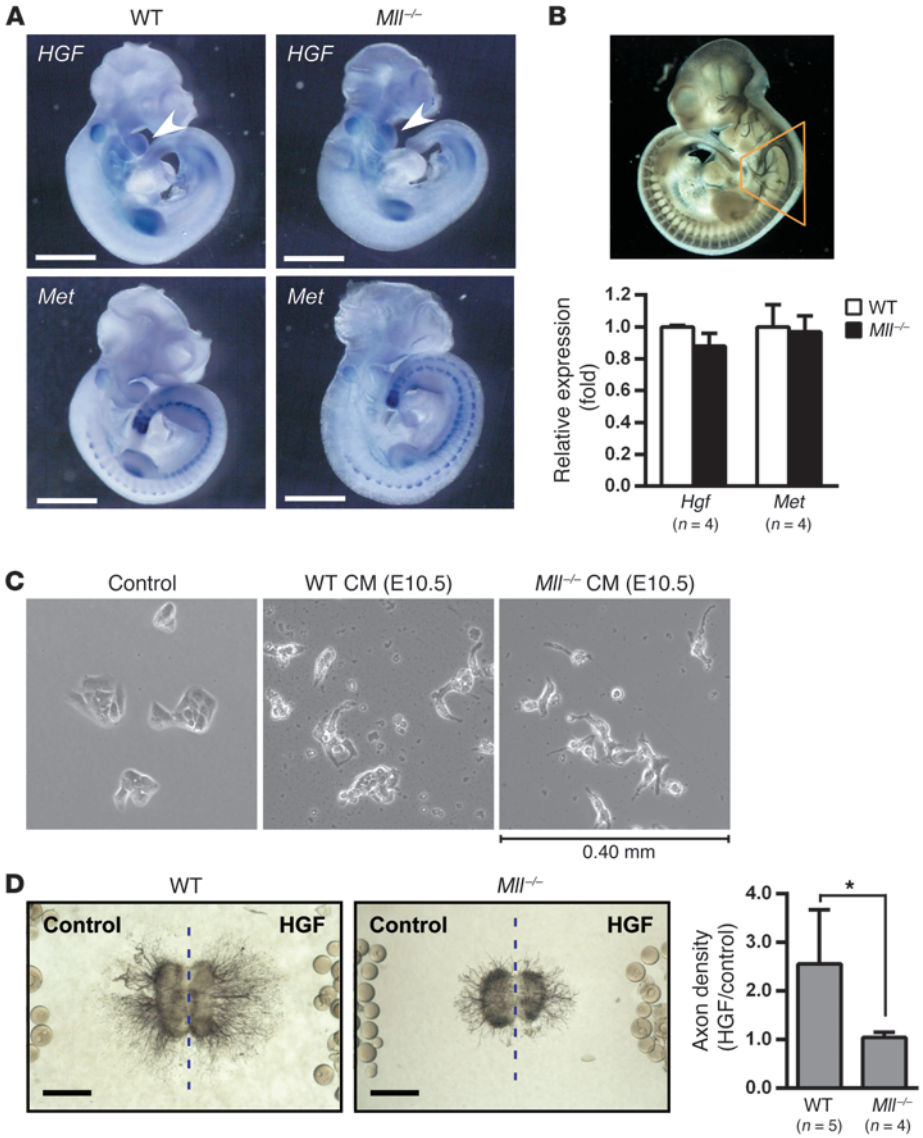

Figure 2
MLL functions downstream of the HGF-MET signaling pathway. (**A**) Whole-mount in situ hybridization analysis of E10.0 WT and *Mll*$^{-/-}$ embryos using specific RNA probes against *Hgf* and *Met* mRNA. No difference in *Hgf* and *Met* expression over the branchial arch region (white arrowhead) was noted. Representative images from 3 independent experiments are shown. Scale bars: 1 mm. (**B**) Quantitative RT-PCR analyses of *Hgf* and *Met* expression in tissues encompassing the hindbrain (orange outline) of WT and *Mll*$^{-/-}$ embryos. Data are mean ± SD. (**C**) MDCK scatter assay demonstrated equal competence of CM derived from WT and *Mll*$^{-/-}$ E10.5 primary MEFs. MDCK cells were allowed to form colonies for 24 hours and incubated in DMEM (Control) or the indicated CM for an additional 24 hours before imaging. (**D**) Ex vivo axon outgrowth assays. Bilateral hindbrain explants of rhombomeres 7 and 8 were cultured in collagen gel for 48 hours in the presence of embedded HGF-soaked and control mock-treated heparin acrylic beads. Explants from *Mll*$^{-/-}$ embryos showed impaired axon outgrowth toward HGF-soaked beads. Axons were immunostained using anti-neurofilament Ab, quantified in binary images using NIH ImageJ, and presented as the ratio of axon density toward HGF-treated versus control beads. Data are mean ± SD. *$P < 0.05$. Scale bars: 0.5 mm.

tal Figure 2). Examinations of the axial skeleton of *Mll*$^{nc/nc}$ newborns revealed increased incidence of homeotic defects, including incomplete segmentation between sternebra 3 and 4 and deformed anterior arch of atlas (a.a.a., C1 vertebra; Supplemental Figure 3, A and B). Neurofilament staining of E10.5 embryos also revealed homeotic defects of CNIX (also known as the glossopharyngeal nerve) in *Mll*$^{nc/nc}$ mice (Supplemental Figure 3C). The homeotic defects we observed in *Mll*$^{nc/nc}$ mice were in accordance with the fact that unprocessed precursor MLL exhibits impaired H3K4 HMT activity (26) and thus functions as a hypomorphic allele.

CNXII outgrowth and myoblast migration defects connect MLL with the HGF-MET signaling pathway. Besides the aforementioned homeotic transformation, a surprising Hox-independent CNXII outgrowth defect was discovered in *Mll*$^{nc/nc}$ embryos (Figure 1A). CNXII innervates and thus controls the movement of tongue muscles. Importantly, such defects were also present in *Tasp1*$^{-/-}$ and *Mll*$^{-/-}$ embryos (Figure 1A), indicating the prerequisite of a fully functional MLL in ensuring the proper outgrowth of CNXII. Remarkably, this phenotype has been observed in both *Hgf*$^{-/-}$ and *Met*$^{-/-}$ mice, but not in any reported Hox gene–knockout mice (33). In addition to CNXII outgrowth defects, *Hgf*$^{-/-}$ and *Met*$^{-/-}$ mice show profound defects in the migration of skeletal myoblasts to limbs, diaphragm, and tongue (34). Accordingly, we investigated whether myoblast migration was affected in *Mll*$^{-/-}$ embryos by in situ hybridization using a *Pax3* probe, which marks migratory myoblasts (35). Interestingly, although migratory myoblasts were present at the forelimbs of *Mll*$^{-/-}$ embryos, they were fewer in number and appeared less organized (Figure 1B). Therefore, substantial overlap of phenotypes between MLL-deficient and HGF-MET–deficient mice was identified, connecting MLL and the HGF-MET signaling pathway. Consequently, we sought to determine whether MLL functions upstream and/or downstream of the HGF-MET pathway.

We first examined whether MLL is required to maintain expression of *Hgf* and *Met* in mouse hindbrain. Whole-mount in situ hybridization and quantitative RT-PCR assays demonstrated comparable transcript levels of *Hgf* and *Met* in the branchial arch and hindbrain region of WT and *Mll*$^{-/-}$ embryos (Figure 2, A and B). HGF functions as a secretory growth factor that was originally cloned based on its

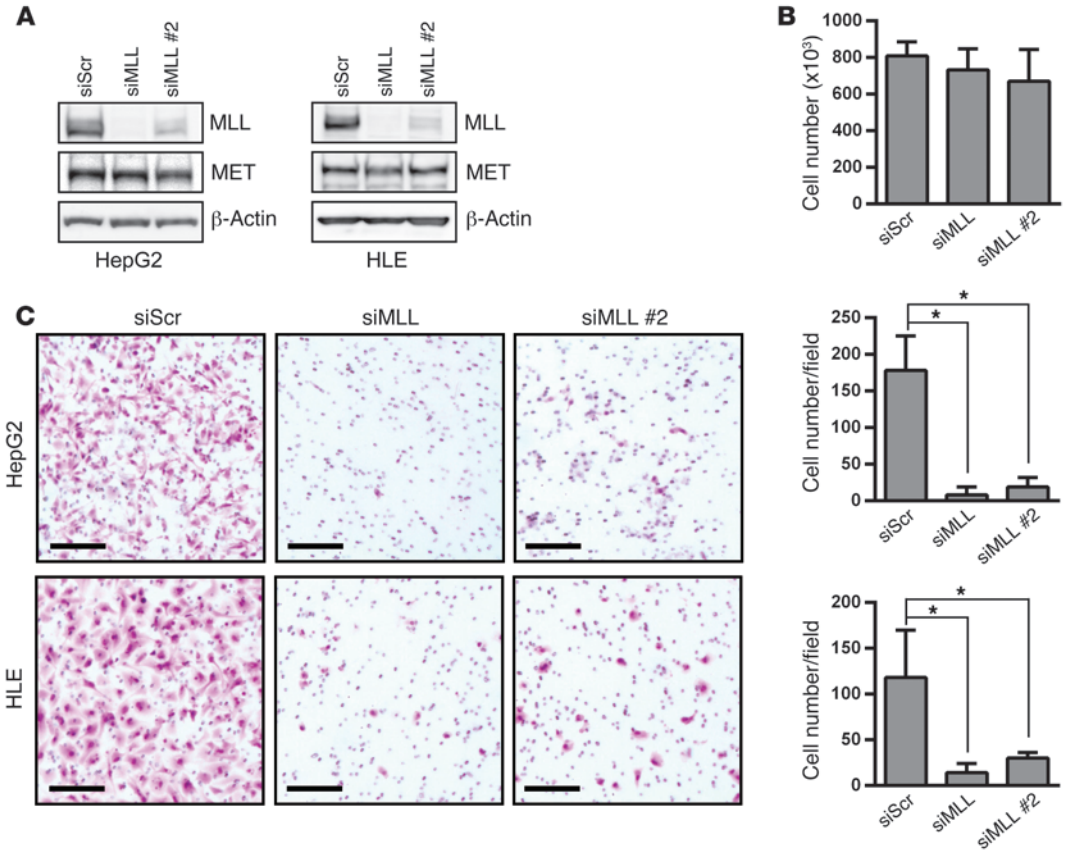

Figure 3

MLL is required for HGF-induced cell invasion. (**A**) siRNA-mediated knockdown of MLL (siMLL and siMLL #2) in HepG2 and HLE cells. Scrambled siRNA (siScr) was used as a control. Anti-MLL Western blot analyses demonstrated effective silencing of MLL. Protein levels of MET in HepG2 and HLE cells transfected with the indicated siRNA oligos were determined by anti-MET Ab. β-actin served as loading control. (**B**) Equivalent numbers of HepG2 cells (4×10^5) carrying the indicated siRNA oligos were cultured for 60 hours to determine their proliferation. (**C**) Cell invasion assay. HepG2 and HLE cells were transfected with the indicated siRNA oligos, seeded on Matrigel-coated transwells, and subjected to 20 and 50 ng/ml HGF, respectively, for 24 hours. Invaded cells were stained with crystal violet and Hoechst 33342. Data are mean ± SD from 5 independent fields of 3 independent experiments. $^*P < 0.05$. Scale bars: 0.2 mm.

activity in dispersing MDCK cells (2, 3). Accordingly, the potency of HGF derived from *Mll*$^{-/-}$ mouse embryonic fibroblasts (MEFs) was assessed by MDCK scatter assay. Conditioned media (CM) derived from WT and *Mll*$^{-/-}$ MEFs displayed comparable capability in scattering MDCK cells (Figure 2C). In summary, MLL deficiency did not affect *Hgf* or *Met* expression, nor HGF activity.

Because HGF is known to promote the axon outgrowth of cranial nerves (32), we therefore investigated the requirement of MLL in HGF-induced axon outgrowth using hindbrain explants. Rhombomeres 7 and 8 were dissected from the hindbrain and embedded in collagen gel along with presoaked HGF or control beads. WT explants showed preferential axon outgrowth toward HGF-soaked beads, whereas *Mll*$^{-/-}$ explants failed to exhibit a notably differential response toward HGF (Figure 2D). Thus, there is an intrinsic requirement of MLL for neurons to respond to HGF-dependent axon outgrowth, indicative of a permissive role of MLL in HGF-MET signal transduction. Collectively, the results of our genetic and functional studies support the notion that MLL functions downstream of the HGF-MET pathway.

MLL is required for HGF-MET to induce cell invasion. To examine the molecular connection between MLL and the HGF-MET signaling pathway, we resorted to an HGF-induced cell invasion assay, using 2 human hepatocellular carcinoma cell lines that express MET and respond to HGF: HepG2 and HLE cells (11, 36). Both HepG2 and HLE cells invaded through Matrigel in response to HGF (Supplemental Figure 4). In line with our genetic studies showing that *Met* expression was not reduced in *Mll*$^{-/-}$ embryos (Figure 2, A and B), knockdown of MLL in hepatocellular carcinoma cells had no apparent effect on protein expression of MET (Figure 3A). Notably, MLL deficiency did not significantly affect cell proliferation within our experimental time frame (Figure 3B). On the other hand, HGF-induced invasion of HepG2 and HLE cells was severely compromised when MLL was depleted (Figure 3C). Taken together, the results of our cell-based invasion assays further support a critical involvement of MLL in the HGF-MET signaling pathway.

MLL deficiency impairs the transcriptional induction of MMP1 and MMP3 upon HGF-MET signaling. Studies over the past 2 decades have outlined the basic signaling framework pertaining to the HGF-MET pathway. It involves an upstream growth factor/RTK pair, HGF-MET; a myriad of intermediary adaptor/signal transduction molecules, such as GAB1, GRB2, and MAPK; several transcription factors, such as AP1 and ETS families; and multiple

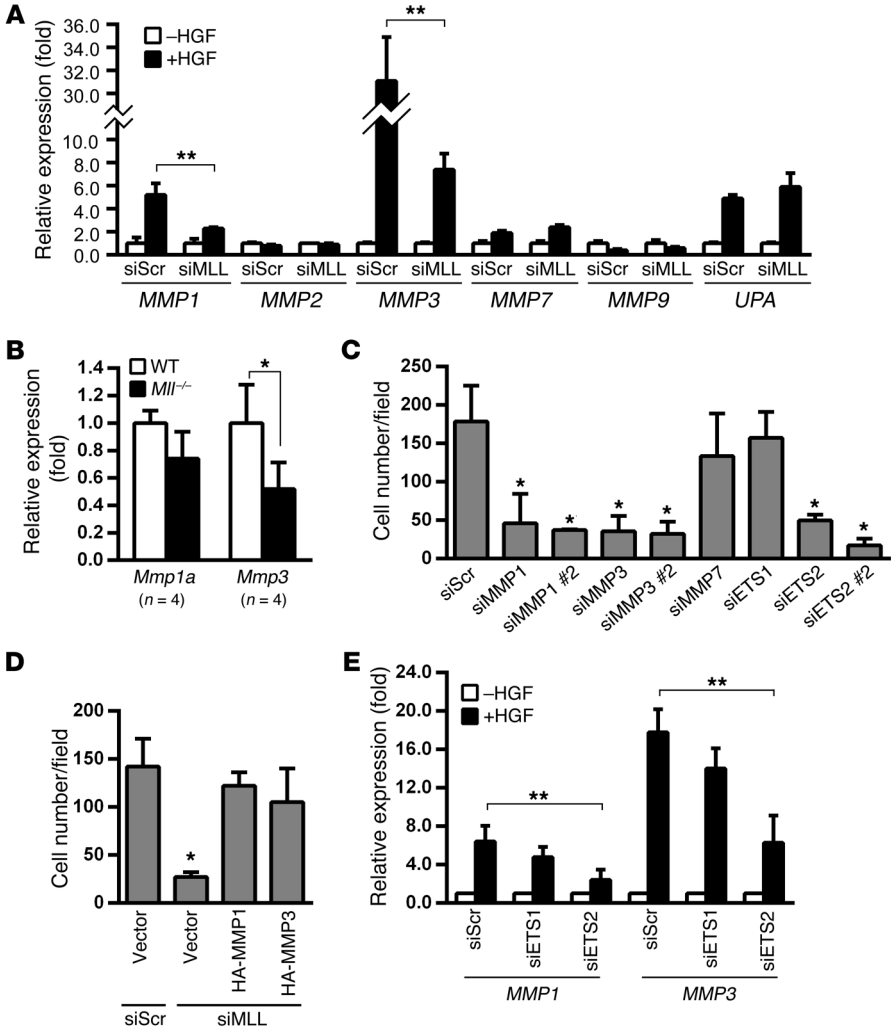

Figure 4
MLL and ETS2 are essential for HGF-induced transactivation of *MMP1* and *MMP3* for cell invasion. (**A**) HepG2 cells transfected with the indicated siRNA oligos were treated with or without HGF for 12 hours, and total RNA was harvested for quantitative RT-PCR analysis for the indicated genes. Transcript levels without HGF treatment were assigned as 1.0. (**B**) Quantitative RT-PCR analyses of *Mmp1a* and *Mmp3* in WT and *Mll*$^{-/-}$ E10.5 mouse hindbrain tissues. (**C**) HepG2 cells transfected with the indicated siRNA oligos were subjected to invasion assays on Matrigel transwells using 20 ng/ml HGF. (**D**) HepG2 cells were cotransfected with the indicated siRNA oligos and constructs expressing HA-tagged MMP1 or MMP3 (or vector control) and subjected to invasion assays using 20 ng/ml HGF. (**E**) Quantitative RT-PCR analysis of *MMP1* and *MMP3* on HepG2 cells transfected with the indicated siRNA oligos in the presence or absence of HGF treatment. Data are mean ± SD from at least 3 independent experiments. *$P < 0.05$; **$P < 0.01$.

downstream effectors, such as uPA and MMPs (4, 37). As MLL is best known as a transcriptional coactivator that enhances transcription, we envisioned that it may directly or indirectly affect the transactivation of certain key HGF-MET target genes. We first focused on MMPs and uPA, which function in remodeling extracellular matrix and breaking down adhesion molecules for cell invasion. Upon HGF treatment, expression of *MMP1*, *MMP3*, *MMP7*, and *UPA* was induced in HepG2 cells, whereas no induction of *MMP2* and *MMP9* was detected (Figure 4A), in agreement with prior reports (11, 38). Among these HGF-inducible genes, induction of *MMP1* and *MMP3*, but not *MMP7* or *UPA*, was significantly blunted in MLL-deficient cells (Figure 4A). Accordingly, expression of *Mmp3* was also decreased in the hindbrain of *Mll*$^{-/-}$ embryos (Figure 4B). We subsequently sought to determine whether MLL-dependent induction of *MMP1* and *MMP3* is necessary for HGF-triggered cell invasion. Indeed, knockdown of MMP1 or MMP3, but not of MMP7, significantly impaired the invasion of HepG2 cells (Figure 4C and Supplemental Figure 5A). Furthermore, MLL-depleted HepG2 cells reconstituted with MMP1 or MMP3 significantly restored their capacity to invade (Figure 4D and Supplemental Figure 5B). Together, our data demonstrated that MLL is required for the proper induction of *MMP1* and *MMP3* by HGF-MET for cell invasion.

HGF-MET signals through ETS2 to transactivate MMP1 and MMP3. Since MLL does not encompass a sequence-specific DNA-binding domain (DB), MLL likely licenses HGF-MET–induced transcription of *MMP1* and *MMP3* through transcription factors. Prior studies of the HGF-MET pathway have recognized ETS1 and ETS2 as key transcription factors that target MMP genes (39). Accordingly, ETS1 and/or ETS2 are prime candidates that collaborate with MLL. We therefore investigated whether ETS1 and/or ETS2 are required for the transactivation of *MMP1* and/or *MMP3*. HepG2 cells with knockdown of ETS1 or ETS2 were treated with HGF, and the transcript levels of *MMP1* and *MMP3* were examined. Deficiency in ETS2 severely compromised induction of *MMP1* and *MMP3* by HGF, whereas deficiency in ETS1 had minor effects (Figure 4E and Supplemental Figure 5, C and D). Notably, endogenous expression of ETS1 in hepatocellular carcinoma cells was low and could not be detectable by commonly used anti-ETS1 Ab. In fact, HepG2 cells deficient in ETS2, but not ETS1, exhibited a marked invasion defect in response to HGF (Figure 4C). These data support the notion that ETS2 functions as the key downstream transcription factor of the HGF-MET signaling pathway to activate MMP1 and MMP3 for the invasion of hepatocellular carcinoma cells.

The HGF-MET signal induces protein expression of ETS2. Thus far, our data demonstrated that both ETS2 and MLL are integral in

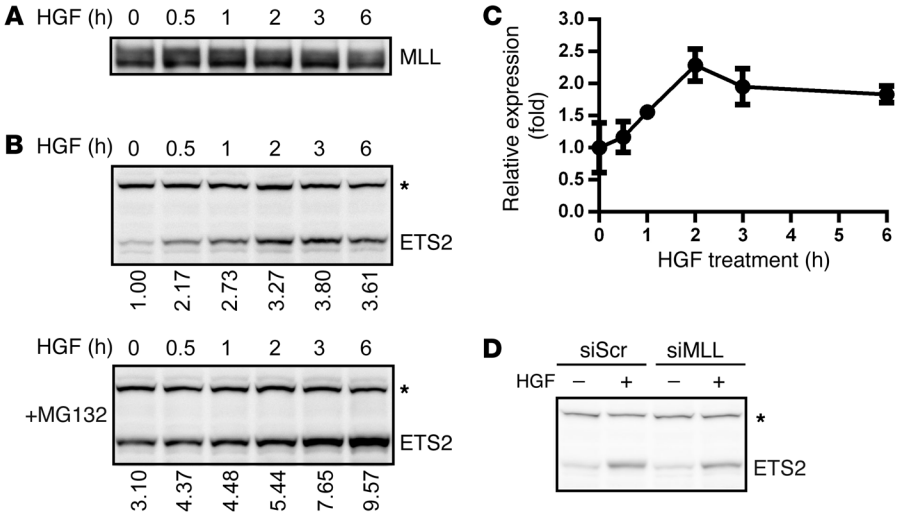

Figure 5

ETS2 protein accumulates upon HGF-MET signaling through blocked degradation and enhanced transcription. (**A**) MLL protein remained constant upon HGF treatment. HepG2 cells were incubated with 20 ng/ml HGF for the indicated times and subjected to anti-MLL^{C180} IB analysis. (**B**) ETS2 protein accumulated upon HGF treatment. HepG2 cells treated with HGF for the indicated times without or with MG132 pretreatment (10 μM for 4 hours) were harvested and subjected to anti-ETS2 IB analysis. Numbers below lanes indicate relative protein levels of ETS2, measured by densitometry and normalized against nonspecific cross-reactive bands (asterisks). (**C**) *ETS2* quantitative RT-PCR on HepG2 cells treated with HGF for the indicated times showed an induction peak at 2 hours. Data are mean ± SD from 3 independent experiments. (**D**) MLL knockdown had no effect on HGF-induced ETS2 accumulation. HepG2 cells transfected with the indicated siRNA oligos were treated with HGF for 3 hours and subjected to anti-ETS2 IB analysis. Asterisk denotes nonspecific cross-reactive band.

the transcriptional induction of *MMP1* and *MMP3* upon HGF-MET signals. However, how HGF-MET signals through MLL and ETS2, and whether MLL and ETS2 function in concert, in parallel, or in sequence to activate *MMP1* and *MMP3*, have yet to be determined. First, we examined whether MLL and/or ETS2 can be induced upon HGF-MET engagement. Interestingly, ETS2 protein was induced approximately 4-fold upon HGF treatment, whereas MLL remained basically unchanged (Figure 5, A and B). We further investigated how HGF-MET activation results in ETS2 accumulation. ETS2 was induced within 30 minutes upon HGF treatment and continued to accumulate over the following 6 hours (Figure 5B). The relatively rapid induction of ETS2 protein (<30 minutes) most likely results from blocked degradation, consistent with our finding that cells pretreated with the proteasome inhibitor MG132 exhibited increased baseline expression of ETS2 protein (3.1-fold; Figure 5B). However, additional mechanisms such as increased transcription must be in place to account for the continuous accumulation of ETS2 observed in the presence of MG132 (Figure 5B). We therefore assessed whether *ETS2* transcript levels increase upon HGF treatment. A approximately 2-fold induction of *ETS2* mRNA was observed at 2 hours after HGF treatment, preceding the peak expression of ETS2 protein at 3 hours (Figure 5, B and C). In summary, HGF-MET enlists ETS2 by disrupting degradation and enhancing transcription. Conversely, no change in MLL protein level was noted in HGF-treated HepG2 cells. We consequently sought to determine whether MLL functions to directly induce ETS2 protein upon HGF-MET activation. No impairment of ETS2 accumulation was observed in MLL-deficient HepG2 cells upon HGF treatment (Figure 5D). Hence, MLL must employ other mechanisms to participate in the HGF-MET pathway.

MLL complexes with and functions as a transcription coactivator of ETS2. As MLL is a transcription coactivator and ETS2 a sequence-specific DNA binding factor, we envisioned that MLL and ETS2 could assemble a transcription complex in hepatocellular carcinoma cells that directly activates *MMP1* and *MMP3*. To examine this hypothesis, co-IP assays were performed. In the absence of HGF, a low but detectable level of MLL was coprecipitated with ETS2, likely due to the scarce amount of ETS2 in untreated HepG2 cells (Figure 6A). Upon HGF treatment, ETS2 was induced and readily complexed with MLL (Figure 6A). Hence, the relative abundance of assembled MLL-ETS2 complex is apparently dictated by the ETS2 protein, which can be induced by active HGF-MET signals. To probe into the function of the MLL-ETS2 complex in gene activation, a GAL4-based luciferase reporter assay was used. A construct consisting of ETS2 fused with the DB of the yeast GAL4 transcription factor (referred to herein as GAL4DB) was transiently coexpressed with or without MLL, and the resulting luciferase activity served as a surrogate for transcription of a GAL4 response element–containing luciferase reporter. The GAL4DB-ETS2 fusion construct activated the GAL4 luciferase reporter approximately 4-fold, which was strongly augmented by coexpressed MLL, resulting in approximately 20-fold induction (Figure 6B).

MLL interacts with the activation domain 2 of ETS2. Our results thus far favored a model in which HGF-MET induces ETS2, which readily complexes with MLL to activate the transcription of *MMP1* and *MMP3*. To provide mechanistic insights as how MLL interacts with ETS2, we performed deletion mapping to identify critical regions of ETS2 required for its association with MLL. Domain compositions have been characterized within the ETS family proteins, including the conserved activation domain 1 (AD1), the pointed domain (PD), the DB, and the diverged activation domain 2 (AD2) (Figure 6C and ref. 40). Co-IP assays using N-terminal deletion mutants of ETS2 demonstrated that deletion of AD1 and PD did not affect MLL-ETS2 interaction, whereas deletion of AD2 in addition to AD1 and PD completely abrogated it (Figure 6C). The importance of AD2 in mediating the MLL-ETS2 interaction was further corroborated when C-terminal deletion mutants were analyzed: deletion of DB had no effect, whereas deletion of DB plus AD2 completely disrupted the interaction (Figure 6C). Since AD2 is the least conserved domain among ETS family proteins (40), it is tempting to speculate that this divergence may contribute to the differential selection of interaction partners by individual ETS transcription factors in response to specific signaling relays.

HGF-MET signals the accumulation of MLL-ETS2 complex at MMP1 and MMP3 promoters. To determine whether the HGF-MET–

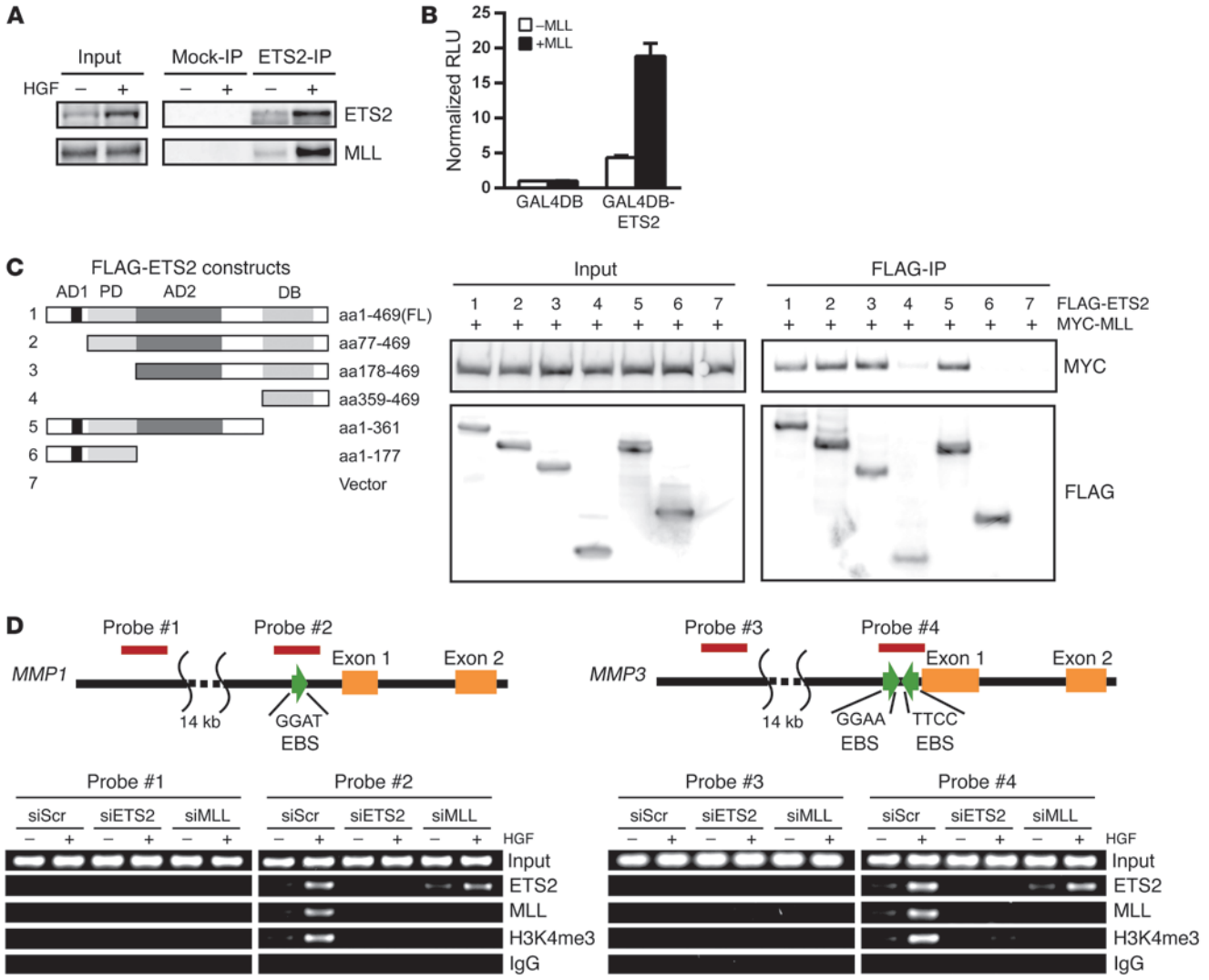

Figure 6

MLL interacts with ETS2 to target the *MMP1* and *MMP3* promoters upon HGF signaling. (**A**) Lysates of HepG2 cells treated with or without HGF for 3 hours were subjected to anti-ETS2 or mock IP and analyzed by Western blot for ETS2 and MLL. (**B**) Luciferase reporter assay. 293T cells were transiently transfected with a luciferase reporter containing GAL4 binding sites, GAL4DB-ETS2 fusion or GAL4DB expression construct, MLL^{C180} or empty vector construct, and a LacZ reporter. Luciferase activities were quantified using a luminometer and normalized against β-galactosidase activity. Data are mean ± SD from 3 independent experiments. (**C**) Deletion mapping co-IP to identify the critical domain in ETS2 for complexing with MLL^{C180}. The domain structures of FLAG-tagged ETS2 constructs used are outlined at left. FL, full-length. 293T cells were cotransfected with MYC-tagged MLL^{C180} and the indicated FLAG-tagged ETS2 deletion mutants. Cell lysates were immunoprecipitated with anti-FLAG M2 agarose beads and analyzed by anti-MYC and anti-FLAG Western blot. (**D**) ChIP assays on *MMP1* and *MMP3* promoters. HepG2 cells transfected with the indicated siRNA oligos were treated with 20 ng/ml HGF for 1 hour and subjected to ChIP assays using ETS2, MLL, and H3K4me3 Abs. IgG served as a control. Precipitated DNA was analyzed by PCR using primers amplifying regions corresponding to an upstream nonregulatory region (probes #1 and #3) and EBSs (probes #2 and #4).

induced MLL-ETS2 complex directly targets promoters of *MMP1* and *MMP3* for gene activation, we performed ChIP assays. Both *MMP1* and *MMP3* promoters contain ETS-binding sites (EBSs) (12, 13). The chromatin association of MLL and ETS2, as well as the H3K4me3 status, at EBSs (probes #2 and #4) and upstream nonregulatory regions (probes #1 and #3) were examined before and after addition of HGF. Prior to treatment, binding of ETS2 to EBSs was barely detectable, whereas HGF markedly increased the occupancy of ETS2 at EBSs (Figure 6D). HGF treatment also induced chromatin association of MLL at EBSs and increased H3K4me3 (Figure 6D). We next sought to determine whether MLL targets EBSs mainly through ETS2. Indeed, MLL failed to accumulate at EBSs upon HGF treatment in ETS2-deficient cells, which concurred with the failed induction of H3K4me3 at *MMP1* and *MMP3* promoters (Figure 6D). In agreement with a model in which MLL targets promoters through accumulated ETS2 upon HGF-MET signals, knockdown of MLL had no effect on HGF-induced ETS2 accumulation at EBSs of *MMP1* and *MMP3* promoters (Figure 6D).

MLL deficiency reduces metastasis of hepatocellular carcinoma cells. Our data thus far demonstrated a critical role for MLL in HGF-

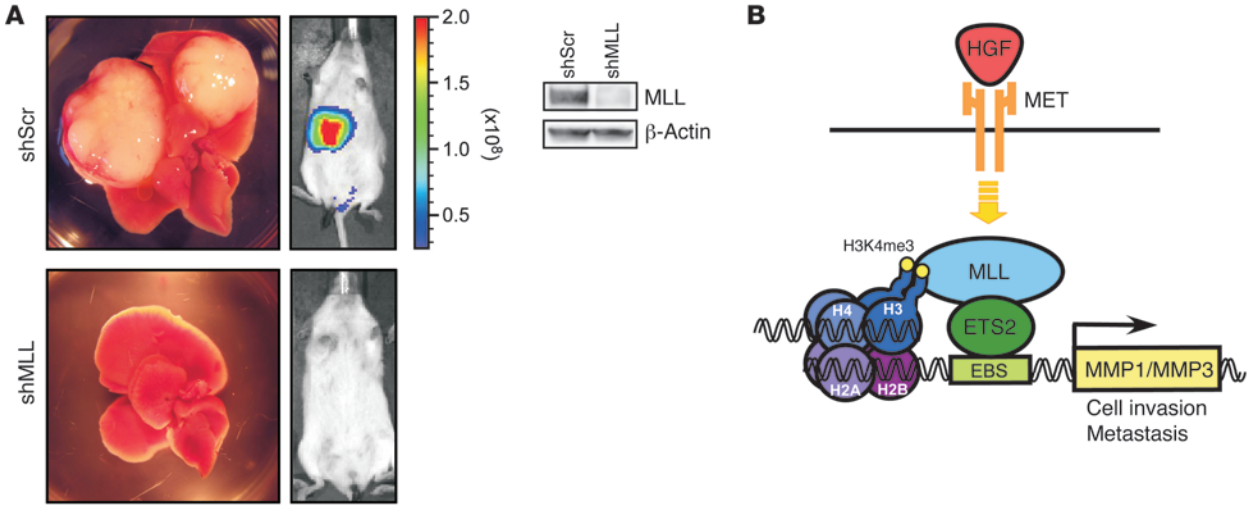

Figure 7

MLL silencing severely compromised metastatic growth of HepG2 cells. (**A**) MLL was stably knocked down in HepG2 cells by retrovirus carrying MLL shRNA in HepG2 cells (right). NSG mice were xenografted with HepG2 cells by tail vein injection. Representative images of livers harvested at necropsy and BLI of xenografted mice are shown (left). Color scale depicts photon flux. shScr, scrambled shRNA control. (**B**) Proposed model by which active HGF-MET signals lead to increased occupancy of the MLL-ETS2 complex on *MMP1* and *MMP3* promoters, where MLL induces H3K4me3, thereby activating target gene expression.

MET–orchestrated cell invasion. Because HGF-MET dysregulation contributes to metastatic phenotypes in various cancers, we investigated whether MLL-deficient liver cancer cells exhibit compromised capacity in metastasis. HepG2 cells stably expressing firefly luciferase were subjected to shRNA-mediated stable knockdown of MLL before xenografting in immunocompromised NOD-SCID *Il2rg*$^{-/-}$ (NSG) mice via tail vein injection. Mice were monitored for tumor metastasis by bioluminescence imaging (BLI) for 6 weeks and then sacrificed for necropsy (Figure 7A). Control HepG2 cells exhibited prevalent metastatic cancer cell growth compared with MLL-deficient HepG2 cells (86% vs. 25%; $P = 0.0195$; Table 1), which confirmed the role of MLL in invasive tumor growth.

Discussion

Homeotic genes of invertebrates and Hox genes of vertebrates encode a family of related transcription-regulatory proteins that play essential roles in implementing developmental patterns and conferring critical positional information (15). Loss of *trithorax* in *Drosophila* and *Mll* in mice incurred global loss of homeotic/Hox gene expression, resulting in profound homeotic defects (41, 42). Hox genes located at the 3′ end of the clusters are expressed earlier and more rostrally during development than those at the 5′ end. Accordingly, deficiency in 3′ Hox genes leads to homeotic defects in the anterior part of the body (43–46). *Mll*$^{nc/nc}$ and *Tasp1*$^{-/-}$ mice exhibit homeotic defects in skeletons and nervous systems (26) that are also observed in mice deficient for *Hoxa3*, *Hoxa4*, or *Hoxa5* (44, 47, 48). This demonstrates the importance of MLL cleavage in regulating the 3′ early Hox genes, resonating with our prior in vitro data showing that knockdown of taspase-1 specifically disrupts the expression of early but not late Hoxa genes (28). Analogous to a noncleaved MLL in mammals, *trx*^{E3} *Drosophila*, in which the taspase-1 cleavage site was genetically deleted, exhibited selectively reduced expression of the 3′ anterior antennapedia (*ANT-C*) homeotic gene, but not the 5′ posterior bithorax (*BX-C*) homeotic gene (41). Interestingly, homeotic defects observed in *Mll*$^{nc/nc}$ mice were less penetrant and less conspicuous than those in *Tasp1*$^{-/-}$ mice, suggestive of potential genetic complementation from other taspase-1 substrates, such as MLL2, TFIIA, and ALF.

Our generation of *Mll*$^{nc/nc}$ animals uncovered a previously unrecognized role of MLL in the HGF-MET signaling pathway. It has been shown that proper outgrowth of CNXII in mouse embryos relies on an intact HGF-MET pathway. HGF is expressed in branchial arches, whereas MET is expressed in subpopulations of cranial motor neurons. HGF has been shown to promote neuronal induction and axon outgrowth and to stimulate Schwann cell proliferation (49). Genetic loss of *Hgf* and *Met* specifically disrupts axonal outgrowth from rhombomeres 7 and 8, therefore impairing the innervation of CNXII (32). Our findings of specific CNXII defects in *Mll*$^{nc/nc}$, *Mll*$^{-/-}$, and *Tasp1*$^{-/-}$ mice support the notion of specialized involvement of MLL in the HGF-MET signaling pathway. Indeed, our axon outgrowth assay using hindbrain explants of rhombomeres 7 and 8 demonstrated a role of MLL in HGF-MET–induced axonal growth. In addition to controlling CNXII outgrowth, HGF and MET also regulate the migration of skeletal

Table 1

Frequencies and sites of metastasis from xenografted HepG2 cells

Metastasis site	shScr	shMLL
Liver	6 of 7 (86%)	2 of 8 (25%)
Lymph node	2 of 7 (29%)	0 of 8 (0%)
Adrenal gland	1 of 7 (14%)	0 of 8 (0%)
Any	6 of 7 (86%)	2 of 8 (25%)

shScr, scrambled shRNA control; shMLL, shRNA-mediated stable MLL knockdown.

myoblasts to limbs, diaphragm, and tongue (34). When the migration of myoblasts to forelimbs was examined, we observed migration defects in *Mll*$^{-/-}$ embryos. Although genetic defects associated with *Mll*$^{-/-}$ embryos were less profound than those of *Hgf*$^{-/-}$ and *Met*$^{-/-}$ embryos, the substantial phenotypic overlap between *Mll*$^{-/-}$ mice and *Hgf*$^{-/-}$ and *Met*$^{-/-}$ mice underscores the underlying genetic linkage between MLL and the HGF-MET signaling pathway.

Our study using hepatocellular carcinoma cell lines demonstrated that MMP1 and MMP3 functioned as key downstream effectors mediating HGF-MET–induced cell invasion, the transcriptional activation of which required MLL and ETS2, but not ETS1. As MLL and ETS2 formed a complex through the less-conserved AD2, this evolved divergence could contribute to the observed specific requirement of ETS2, but not ETS1, for HGF-induced transcription of *MMP1* and *MMP3*. Therefore, ETS1 and ETS2 are more likely functionally distinct than redundant, a notion supported by prior studies in mice deficient in individual ETS genes. *Ets2*$^{-/-}$ mice die at E8.5 due to defects in trophoblast migration, whereas *Ets1*$^{-/-}$ mice are viable and grossly normal, except for reduced T cell numbers (50). Along the same line, it has been proposed that ETS2, but not ETS1, functions as the critical downstream transcription factor that signals downstream to PTEN loss in facilitating mammary epithelial tumorigenesis (51).

HGF-MET induced the activity of ETS2 via deterred protein degradation and enhanced transcription. This HGF-MET–induced ETS2 accumulation ultimately led to assembly of the ETS2-MLL complex on *MMP1* and *MMP3* promoters. ChIP assays demonstrated minimal EBS association of ETS2 and MLL before treatment with HGF, consistent with the low level of ETS2 protein present in hepatocellular carcinoma cells prior to HGF-MET signal activation. Knockdown of ETS2 affected the targeting of MLL onto the EBSs of *MMP1* and *MMP3*, whereas knockdown of MLL had no effects on ETS2 binding. Hence, ETS2 is primarily responsible for directing the ETS2-MLL complex to the respective promoters. Although detailed molecular mechanisms concerning stability, transcription, and DNA binding of ETS2 remain to be determined, our results uncovered an ETS2-centered molecular switch whereby HGF-MET signals the increase of ETS2 protein, which results in accumulation of the ETS2-MLL complex that targets EBSs through ETS2 and methylates H3K4 through its MLL moiety, ultimately leading to activation of MMP1 and MMP3 for cell invasion (Figure 7B).

The HGF-MET signaling pathway plays an essential role in diverse developmental processes, and its dysregulation contributes to invasion and metastasis phenotypes of human cancers (4, 52). Like the other RTKs, MET has been targeted for anticancer therapies using chemical inhibitors and antagonizing peptides and/or Abs (25). However, human malignancies with dysregulated RTK eventually become resistant to targeted therapies due to acquired mutations in the receptor itself or in downstream signaling components. Therefore, further understanding of the molecular details downstream of the HGF-MET pathway may present additional anticancer therapeutic strategies. Here, we revealed a novel HGF-MET–enhanced ETS2-MLL complex that directly activated *MMP1* and *MMP3* transcription for the invasion of hepatocellular carcinoma cells. Since MLL mainly enhances transcription through its HMT activity, inhibitors of its HMT may offer specific measures by which to interfere with MMP1 and MMP3 induction, thereby deterring the invasiveness of cancers driven by hyperactive HGF-MET signals. Furthermore, as taspase-1–mediated cleavage of MLL was required for full HMT activity of MLL, inhibition of taspase-1 may render an alternative treatment strategy.

Besides the HGF-MET pathway, EGF, VEGF, and bFGF have been reported to function upstream of ETS1 and ETS2 transcription factors (53–55). These signaling pathways promote cell invasion in a remarkably similar fashion, in which MMP expression is activated via ETS transcription factors. For example, EGF transiently induces protein levels of ETS1 and ETS2 and the ensuing upregulation of MMP1, MMP9, and uPA in SK-BR3 breast cancer cells (53). Given the critical role of MLL in HGF-MET signaling and the sharing of some downstream signaling components among different growth factor signaling pathways, MLL family proteins may participate in other growth factor signaling pathways beyond the present study. Future investigation of the potential involvement of MLL and its family members in individual growth factor signaling pathways may shed additional light on the epigenetic control of RTK signaling beyond HGF-MET.

Methods

Mice. The genomic DNA coding sequences for cleavage sites 1 and 2 of MLL were replaced by PCR-mediated site-directed mutagenesis. The targeting construct was fully sequenced and introduced into Rw4 ES cells, a male 129/svJ ES line, through homologous recombination. Individual clones carrying the noncleavable allele were verified by Southern and Western analyses. Transient expression of Cre recombinase was performed to delete the Neo cassette. Clones with correct recombination and normal karyotype were injected into C57BL/6 blastocysts. Males with high chimerism were mated with C57BL/6 females. Successful germline transmission of the mutant allele was confirmed by PCR. Primer sequences were as follows: forward, GACACGGTAAGTGATGTGCAGC; reverse, CTGCAGTTCCCGTCAAACTGTG. *Mll*$^{nc/+}$ mice were backcrossed with C57BL/6 mice for 10 generations before intercrossing to generate *Mll*$^{nc/nc}$ mice for analysis. *Mll*$^{+/-}$ and *Tasp1*$^{+/-}$ mice in pure C57BL/6 background exhibited sterility issues. *Mll*$^{+/-}$ mice have been described previously (18) and were maintained on the CD1 genetic background. *Tasp1*$^{+/-}$ mice were backcrossed with C57BL/6 mice for 6 generations and maintained by intercross (26).

Skeletal studies and whole-mount immunohistochemistry. Skeletal studies were performed as previously described (26). Whole-mount immunohistochemistry of neurofilament was performed on E10.5 mouse embryos; data presented were based on analysis at somite #36. Embryos were fixed with 4% PFA in PBS overnight, bleached using 6% H_2O_2 in methanol, and dehydrated in 100% methanol. Samples were blocked in 5% FCS and 1% Triton-X100 in PBS, then incubated with neurofilament-specific 2H3 mouse mAb (Developmental Studies Hybridoma Bank). Following incubation with peroxidase-conjugated anti-mouse IgG, staining was visualized with 4-chloro-1-naphtol. Stained embryos were photographed under a stereoscopic microscope (Zeiss), and the distance from the end of CNXII to the intersection point between CNX and CNXII was measured.

In situ hybridization. For in situ hybridization, embryos were fixed with 4% PFA in PBS, cryoprotected in 20% sucrose in PBS, frozen in OCT Compound (Tissue-Tek), and sectioned. The template for *Pax3* RNA probe was constructed based on NCBI probe database (Pr196191.1). Serial sections were thaw mounted on Superfrost Plus slides (Thermo Fisher Scientific). Slides were fixed using 4% PFA in PBS, permeabilized with proteinase K, postfixed using 4% PFA in PBS, and washed in 0.1M triethanolamine-HCl with 0.25% acetic anhydride. Hybridization was performed overnight at 65°C with digoxigenin-labeled (DIG-labeled) cRNA probes in hybridization buffer. Slides were washed in 2× SSC at 61°C, washed in 0.2× SSC at 65°C, blocked with 10% sheep serum in PBS, and incubated with alkaline phosphatase–labeled (AP-labeled) anti-DIG Fab fragments (Roche) overnight. After sec-

tions were washed, staining was visualized using nitro blue tetrazolium and 5-bromo-4-chloro-3-indolyl phosphate (Roche). Sections were coverslipped in 90% glycerol with Vectashield Mounting Medium (Vector Laboratories).

Whole-mount in situ hybridization was performed on E10.0 mouse embryos (somites #28–#32). The templates for *Hgf* and *Met* RNA probes were provided by C. Birchmeier (Max Delbrück Center for Molecular Medicine, Berlin, Germany). Embryos were fixed with 4% PFA in PBS, permeabilized with proteinase K, and then postfixed with 4% PFA and 0.2% glutaraldehyde in PBS. Hybridization was performed overnight at 65°C with DIG-labeled RNA probes in hybridization buffer (50% formamide, 5× SSC, 0.3 mg/ml yeast RNA, 0.1 mg/ml heparin, 1× Denhardt's, 0.1% Tween 20, and 5 mM EDTA). Embryos were washed, blocked in 10% sheep serum in TBST (250 mM Tris-HCl, 750 mM NaCl, 50 mM KCl, and 1% Tween 20), and incubated overnight at 4°C with AP-conjugated anti-DIG Fab fragments. After extensive washes, color reaction was carried out using BM purple (Roche).

Hindbrain explant culture and axon outgrowth assay. Hindbrain explants at rhombomeres 7 and 8 were obtained from E10.0 embryos. Bilateral hindbrain tissues containing the whole floor plate and the ventral half of neuroepithelium were dissected in ice-cold HBSS (Invitrogen). Collagen gel was generated as a mixture of equal volumes rat tail collagen (Fisher), Matrigel matrix (BD), and DMEM (Invitrogen). Heparin-acrylic beads (Sigma-Aldrich) were incubated in HBSS containing 200 ng/μl mouse recombinant HGF (R&D Systems) or HBSS alone for 3 hours at room temperature. Hindbrain tissues were embedded in the collagen gel with laterally placed clusters of 10–20 beads at a distance of 500–750 μm and cultured in medium consisting of 75% OptiMEM (Invitrogen) and 25% F12 supplemented with 5% FBS, 40 mM glucose, and 1× penicillin/streptomycin. After 48 hours of culture, explants were fixed with 4% PFA and immunostained using anti-neurofilament 2H3 Ab. Stained axons were visualized with 4-chloro-1-naphtol and photographed under a stereoscopic microscope (Zeiss). For quantification, images of stained axons were processed to binary images using NIH ImageJ, as described previously (56). The proportion of the area covered by axons in lateral square areas adjacent to hindbrain explants was quantified by ImageJ.

Plasmid construction. The MLL^{C180} cDNA was cloned in-frame into the expression vector CMV-MYC (Clontech). cDNAs expressing MMP1 and MMP3 were cloned into CMV-HA (Clontech). cDNAs encoding full-length and deletion mutants of ETS2 were cloned into an pCMV-3xFLAG (Sigma-Aldrich) for IP assay, or into a GAL4DB (aa 1–147) expression vector (GH250) for luciferase reporter assays.

siRNA oligos. siRNA oligos were as follows: siMLL, GGAGUGUAAUAAGUGCCGA; siMLL #2, GTAACAACTATCAGAATCT; siMMP1, CCAACAAUUUCAGAGAGUA; siMMP1 #2, GGAAUUCUUUGGGCUGAAA; siMMP3, GAGAUUUGAUGAGAAGAGA; siMMP3 #2, CAGUUGGAGUUUGACCCAA; siMMP7, GAAUACUCACUAUUUCCAA; siMMP7 #2, CGAUUAGUGUCAAAGGCUU; siETS1, GCAUUAAAAGCUACUUUCA; siETS1 #2, GCCUGAAAGGUGUAGACUU; siETS2, GACAGAAGAUCAAUAUGAA; siETS2 #2, GAGACGGAUGGGAGUUUA.

Cell culture and transfection. HepG2, MDCK, and 293T cells were purchased from ATCC, and HLE cells were purchased from the Health Science Research Resources Bank. Cells were maintained in DMEM supplemented with 10% fetal bovine serum, nonessential aas, L-glutamine, and penicillin/streptomycin. Constructs were transfected in 293T cells using Lipofectamine 2000 (Invitrogen) according to the manufacturer's instructions. Oligos, Silencer Select siRNA oligos (Applied Biosciences), and siGENOME oligos (Dharmacon) were transfected into HepG2 and HLE cells by reverse transfection using lipofectamine RNAiMAX (Invitrogen) according to the manufacturer's instructions. Cells were incubated with siRNA for 48 hours before being subjected to assays.

MDCK cell scatter assay. 1×10^4 MDCK cells were plated on a 12-well plate and cultured for 24 hours to allow for the formation of discrete colonies. MDCK cells were then cultured for an additional 24 hours in the presence of CM harvested from primary MEF culture.

Cell invasion assay. 5×10^4 HepG2 or HLE cells were plated on a BioCoat Matrigel-coated transwell with 8-μm pores (BD Biosciences). Medium in the lower compartment was supplemented with 20 ng/ml (HepG2) or 50 ng/ml (HLE) human recombinant HGF (Sigma-Aldrich). Following 24 hours of culture, cells attached to the upper side of the transwell were mechanically removed with cotton swabs. Cells that invaded to the lower side were fixed with formalin and stained with crystal violet (Fisher) and Hoechst 33342 (Invitrogen) for quantification. 5 independent fields per transwell were photographed under a microscope, and the number of invaded cells in every field was counted. Each assay was independently performed at least 3 times.

Abs, IB analysis, and IP. The anti-MLL^{C180} Ab has been described previously (28). The anti-ETS2 Ab (MO526) was generated by immunizing rabbits against the peptide encompassing aa 1–70 of human ETS2. Commercially available Abs used in this study were as follows: anti-MET (sc161; Santa Cruz), anti–β-actin (AC-15; Sigma-Aldrich), anti-MYC (9E10; Santa Cruz), anti-FLAG (M2; Sigma-Aldrich), anti-HA (12CA5), anti-ETS1 (sc350; Santa Cruz), anti-ETS2 (sc22803; Santa Cruz), anti-GAL4DB (sc510; Santa Cruz), anti-H3K4me3 (ab8580; Abcam). Cells or embryos were lysed in RIPA buffer supplemented with Complete protease inhibitors (Roche). Lysates were loaded to NuPAGE gels (Invitrogen) and transferred onto PVDF (Immobilon-P; Millipore). Proteins of interest were detected by the indicated Abs and enhanced chemiluminescence reagents (Western Lightening; Perkin Elmer) using LAS-300 Imaging system (FUJIFILM Life Science). IP assays were performed as previously described (26).

Luciferase reporter assay. 293T cells were transiently transfected with 100 ng pGL2-GAL4-Luciferase vector (Promega), 100 ng *lacZ*-expressing CH110 (Pharmacia), 25 ng GAL4DB-ETS2 construct, and 1,500 ng MYC-MLL^{C180} construct using Lipofectamine 2000 (Invitrogen). Cells were harvested and lysed in cell lysis buffer (BD Biosciences) at 24 hours after transfection. Cell lysates were assayed for luciferase activity using Enhanced Luciferase Assay Kit (BD Biosciences). Data were acquired using a luminometer and normalized for transfection efficiency based on β-galactosidase activity.

ChIP assay. ChIP assays were performed as described previously (21). In brief, HepG2 cells treated with HGF or mock treated for 1 hour were fixed, lysed, and sonicated. IP was performed using specific Abs against ETS2, MLL^{C180}, and H3K4me3. Associated DNA was amplified by PCR with primers recognizing the upstream sequences of the *MMP1* locus.

Primer sequences for probe #1 (human *MMP1* 15 kb upstream) were CCACATGGGCACATTGGA (forward) and CAACAAAAGTTTAATGAGCATCGACTA (reverse). Primer sequences for probe #2 (human *MMP1* EBS) were GCTAGGAGTCACCATTTCTAATGATTG (forward) and GGAAGCTCCCTCTGTATATATAGAGTC (reverse). Primer sequences for probe #3 (human *MMP3* 15 kb upstream) were GAGATTACATAGGGCTAGGAG (forward) and GTGTTGGGATTAGTCAAGTG (reverse). Primer sequences for probe #4 (human *MMP3* EBS) were TCCAGTTTTCTCCTCTACCAAGAC (forward) and GCTTTCATCCAAATGGCAGC (reverse).

Quantitative RT-PCR. Total RNA from mouse tissues or HepG2 cells was extracted using TRIzol reagent (Invitrogen) according to the manufacturer's instruction. For analyses of gene expression in mouse embryos, E10.0 embryo tissues containing the hindbrain, the third branchial arch, and the fourth branchial arch were isolated by excising from the bottom end of the second branchial arch to the top edge of the forelimb bud. RNA was reverse transcribed by Superscript II (Invitrogen) using oligo-dT (Invitrogen) and random decamer primers (Ambion). Quantitative RT-PCR was performed using SYBR green master mix (Applied Biosystems) and gene-specific

primers by ABI Prism 7300 sequence detection system (Applied Biosystems). Gene expression data were normalized against *GAPDH*, detected using GAPDH Taqman probe (Applied Biosystems).

Mouse primer sequences were as follows: *Hgf* forward, GGTTTGGCCATGAATTTGACCTCTATG; *Hgf* reverse, CTGAGGAATGTCACAGACTTCGTAGC; *Met* forward, TACGGACCCAACCATGAGCAC; *Met* reverse, CTTCTGACGTCCCTAGATTAGCAATGG; *Mmp1a* forward, CTATTTCAAAGGCAGCAAAGTATGG; *Mmp1a* reverse, GTCTCTTCCTCACAAACAGCAG; *Mmp3* forward, CACAGACTTGTCCCGTTTCCATCTC; *Mmp3* reverse, GAGGGTGCTGACTGCATCAAAGAAC.

Human primer sequences were as follows: *MLL* forward, CAGCCATTTGCTACGCTACCG; *MLL* reverse, TCAGTAAGAACTGGTGGATCAGGTC; *MMP1* forward, CTTCAAGCCCATTTGGCAGTTGTG; *MMP1* reverse, GCCTTCCAACTCTGGAGTAATGTCAC; *MMP2* forward, GCTCAGATCCGTGGTGAGATCTTC; *MMP2* reverse, GGTGCTGGCTGAGTAGATCCA; *MMP3* forward, TGGCATTCAGTCCCTCTATGGAC; *MMP3* reverse, AGGACAAAGCAGGATCACAGTTGG; *MMP7* forward, GCTGACATCATGATTGGCTTTGCG; *MMP7* reverse, CTGCATTAGGATCAGAGGAATGTCCC; *MMP9* forward, GGGCTACGTGACCTATGACATCC; *MMP9* reverse, TGTATCCGGCAAACTGGCTCC; *UPA* forward, GCTTGTCCAAGAGTGCATGGT; *UPA* reverse, AGGGCTGGTTCTCGATGGT; *ETS1* forward, GTTAATGGAGTCAACCCAGCCTATCC; *ETS1* reverse, GGGGTGACGACTTCTTGTTTGATAGC; *ETS2* forward, CTGACTTTGTGGGTGACATTCTCTGG; *ETS2* reverse, GGAACGGAGGTGAGGTGTGAATTTTC.

Metastasis mouse model and BLI. To generate HepG2 cell lines for xenograft, we first retrovirally introduced firefly luciferase by pMSCVhyg expression vector. After hygromycin selection, infected cells were further infected with shRNA-expressing pSuper retrovirus with puromycin selection markers (OligoEngine), followed by puromycin selection. Targeting sequences of shRNAs were described previously (16). For xenograft, 5×10^5 HepG2 cells were resuspended in 0.1 ml PBS and injected into tail veins of 6-week-old NSG female mice (The Jackson Laboratory) using 25-gauge needles. Tumor metastasis was monitored by weekly BLI. For BLI, mice were anesthetized and intraperitoneally injected with 1.5 mg D-luciferin (Perkin Elmer). Imaging was completed with Xenogen imaging system IVIS200 and analyzed with Living Image software (Xenogen). 6 weeks after xenografting, mice were sacrificed, and tissues were procured and photographed.

Statistics. Results are presented as mean ± SD unless otherwise specified. Significance of differences was determined by unpaired 2-tailed Student's *t* test, except for mouse metastasis incidence (Fisher exact test). A *P* value less than 0.05 was considered significant.

Study approval. All animal work was performed in accordance with a protocol approved by the IACUC of Memorial Sloan-Kettering Cancer Center.

Acknowledgments

We apologize to the investigators whose research could not be appropriately cited because of space limitations. We thank Carmen Birchmeier for providing the probes for *Hgf* and *Met*; Paul Gray for technical assistance and invaluable suggestions; and Raphael Kopan, Gregory Longmore, and David Ornitz for insightful discussions. P.A. Trainor is supported by the Stowers Institute. This work was supported by NIH grants CA119008 and CA138505 and by a Scholar Award of the American Cancer Society to J.J. Hsieh.

Received for publication July 5, 2012, and accepted in revised form March 29, 2013.

Address correspondence to: James J. Hsieh, Human Oncology and Pathogenesis Program, Memorial Sloan-Kettering Cancer Center, 1275 York Ave., New York, New York 10065, USA. Phone: 646.888.3263; Fax: 646.888.3266; E-mail: hsiehj@mskcc.org.

1. Lemmon MA, Schlessinger J. Cell signaling by receptor tyrosine kinases. *Cell*. 2010;141(7):1117–1134.
2. Stoker M, Gherardi E, Perryman M, Gray J. Scatter factor is a fibroblast-derived modulator of epithelial cell mobility. *Nature*. 1987;327(6119):239–242.
3. Nakamura T, et al. Molecular cloning and expression of human hepatocyte growth factor. *Nature*. 1989;342(6248):440–443.
4. Birchmeier C, Birchmeier W, Gherardi E, Vande Woude GF. Met, metastasis, motility and more. *Nat Rev Mol Cell Biol*. 2003;4(12):915–925.
5. Nelson CM, Bissell MJ. Of extracellular matrix, scaffolds, and signaling: tissue architecture regulates development, homeostasis, and cancer. *Annu Rev Cell Dev Biol*. 2006;22:287–309.
6. Kessenbrock K, Plaks V, Werb Z. Matrix metalloproteinases: regulators of the tumor microenvironment. *Cell*. 2010;141(1):52–67.
7. Dunsmore SE, Rubin JS, Kovacs SO, Chedid M, Parks WC, Welgus HG. Mechanisms of hepatocyte growth factor stimulation of keratinocyte metalloproteinase production. *J Biol Chem*. 1996;271(40):24576–24582.
8. Rosenthal EL, Johnson TM, Allen ED, Apel IJ, Punturieri A, Weiss SJ. Role of the plasminogen activator and matrix metalloproteinase systems in epidermal growth factor- and scatter factor-stimulated invasion of carcinoma cells. *Cancer Res*. 1998;58(22):5221–5230.
9. Hanzawa M, et al. Hepatocyte growth factor upregulates E1AF that induces oral squamous cell carcinoma cell invasion by activating matrix metalloproteinase genes. *Carcinogenesis*. 2000;21(6):1079–1085.
10. Daniels JT, Limb GA, Saarialho-Kere U, Murphy G, Khaw PT. Human corneal epithelial cells require MMP-1 for HGF-mediated migration on collagen I. *Invest Ophthalmol Vis Sci*. 2003;44(3):1048–1055.
11. Ozaki I, et al. Induction of multiple matrix metalloproteinase genes in human hepatocellular carcinoma by hepatocyte growth factor via a transcription factor Ets-1. *Hepatol Res*. 2003;27(4):289–301.
12. Gutman A, Wasylyk B. The collagenase gene promoter contains a TPA and oncogene-responsive unit encompassing the PEA3 and AP-1 binding sites. *EMBO J*. 1990;9(7):2241–2246.
13. Wasylyk C, Gutman A, Nicholson R, Wasylyk B. The c-Ets oncoprotein activates the stromelysin promoter through the same elements as several non-nuclear oncoproteins. *EMBO J*. 1991;10(5):1127–1134.
14. Gum R, et al. Stimulation of 92-kDa gelatinase B promoter activity by ras is mitogen-activated protein kinase kinase 1-independent and requires multiple transcription factor binding sites including closely spaced PEA3/ets and AP-1 sequences. *J Biol Chem*. 1996;271(18):10672–10680.
15. Krumlauf R. Hox genes in vertebrate development. *Cell*. 1994;78(2):191–201.
16. Liu H, Cheng EH, Hsieh JJ. Bimodal degradation of MLL by SCFSkp2 and APCCdc20 assures cell cycle execution: a critical regulatory circuit lost in leukemogenic MLL fusions. *Genes Dev*. 2007;21(19):2385–2398.
17. Krivtsov AV, Armstrong SA. MLL translocations, histone modifications and leukaemia stem-cell development. *Nat Rev*. 2007;7(11):823–833.
18. Yu BD, Hess JL, Horning SE, Brown GA, Korsmeyer SJ. Altered Hox expression and segmental identity in Mll-mutant mice. *Nature*. 1995;378(6556):505–508.
19. Jude CD, Climer L, Xu D, Artinger E, Fisher JK, Ernst P. Unique and independent roles for MLL in adult hematopoietic stem cells and progenitors. *Cell Stem Cell*. 2007;1(3):324–337.
20. Liu H, Takeda S, Cheng EH, Hsieh JJ. Biphasic MLL takes helm at cell cycle control: Implications in human mixed lineage leukemia. *Cell cycle*. 2008;7(4):428–435.
21. Liu H, et al. Phosphorylation of MLL by ATR is required for execution of mammalian S-phase checkpoint. *Nature*. 2010;467(7313):343–346.
22. Liedtke M, Cleary ML. Therapeutic targeting of MLL. *Blood*. 2009;113(24):6061–6068.
23. Milne TA, et al. MLL targets SET domain methyltransferase activity to Hox gene promoters. *Mol Cell*. 2002;10(5):1107–1117.
24. Mohan M, Lin C, Guest E, Shilatifard A. Licensed to elongate: a molecular mechanism for MLL-based leukaemogenesis. *Nat Rev*. 2010;10(10):721–728.
25. Cecchi F, Rabe DC, Bottaro DP. Targeting the HGF/Met signalling pathway in cancer. *Eur J Cancer*. 2010;46(7):1260–1270.
26. Takeda S, et al. Proteolysis of MLL family proteins is essential for taspase1-orchestrated cell cycle progression. *Genes Dev*. 2006;20(17):2397–2409.
27. Tyagi S, Chabes AL, Wysocka J, Herr W. E2F activation of S phase promoters via association with HCF-1 and the MLL family of histone H3K4 methyltransferases. *Mol Cell*. 2007;27(1):107–119.
28. Hsieh JJ, Cheng EH, Korsmeyer SJ. Taspase1: a threonine aspartase required for cleavage of MLL and proper HOX gene expression. *Cell*. 2003;115(3):293–303.
29. Yokoyama A, et al. Proteolytically cleaved MLL subunits are susceptible to distinct degradation pathways. *J Cell Sci*. 2011;124(pt 13):2208–2219.
30. Zhou H, et al. Uncleaved TFIIA is a substrate for taspase 1 and active in transcription. *Mol Cell Biol*. 2006;26(7):2728–2735.
31. Capotosti F, Hsieh JJ, Herr W. Species selectivity of Mixed Lineage Leukemia/Trithorax and HCF proteolytic maturation pathways. *Mol Cell Biol*. 2007;27(20):7063–7072.
32. Caton A, et al. The branchial arches and HGF are growth-promoting and chemoattractant for cranial

motor axons. *Development*. 2000;127(8):1751–1766.
33. Cordes SP. Molecular genetics of cranial nerve development in mouse. *Nat Rev Neurosci*. 2001; 2(9):611–623.
34. Bladt F, Riethmacher D, Isenmann S, Aguzzi A, Birchmeier C. Essential role for the c-met receptor in the migration of myogenic precursor cells into the limb bud. *Nature*. 1995;376(6543):768–771.
35. Goulding M, Lumsden A, Paquette AJ. Regulation of Pax-3 expression in the dermomyotome and its role in muscle development. *Development*. 1994; 120(4):957–971.
36. Jiang Y, Xu W, Lu J, He F, Yang X. Invasiveness of hepatocellular carcinoma cell lines: contribution of hepatocyte growth factor, c-met, and transcription factor Ets-1. *Biochem Biophys Res Commun*. 2001; 286(5):1123–1130.
37. Rosario M, Birchmeier W. How to make tubes: signaling by the Met receptor tyrosine kinase. *Trends Cell Biol*. 2003;13(6):328–335.
38. Tacchini L, Dansi P, Matteucci E, Desiderio MA. Hepatocyte growth factor signalling stimulates hypoxia inducible factor-1 (HIF-1) activity in HepG2 hepatoma cells. *Carcinogenesis*. 2001;22(9):1363–1371.
39. Westermarck J, Kahari VM. Regulation of matrix metalloproteinase expression in tumor invasion. *FASEB J*. 1999;13(8):781–792.
40. Schneikert J, Lutz Y, Wasylyk B. Two independent activation domains in c-Ets-1 and c-Ets-2 located in non-conserved sequences of the ets gene family. *Oncogene*. 1992;7(2):249–256.
41. Breen TR. Mutant alleles of the Drosophila trithorax gene produce common and unusual homeotic and other developmental phenotypes. *Genetics*. 1999;152(1):319–344.
42. Hanson RD, et al. Mammalian Trithorax and polycomb-group homologues are antagonistic regulators of homeotic development. *Proc Natl Acad Sci U S A*. 1999;96(25):14372–14377.
43. Condie BG, Capecchi MR. Mice homozygous for a targeted disruption of Hoxd-3 (Hox-4.1) exhibit anterior transformations of the first and second cervical vertebrae, the atlas and the axis. *Development*. 1993;119(3):579–595.
44. Horan GS, Wu K, Wolgemuth DJ, Behringer RR. Homeotic transformation of cervical vertebrae in Hoxa-4 mutant mice. *Proc Natl Acad Sci U S A*. 1994; 91(26):12644–12648.
45. Barrow JR, Capecchi MR. Targeted disruption of the Hoxb-2 locus in mice interferes with expression of Hoxb-1 and Hoxb-4. *Development*. 1996; 122(12):3817–3828.
46. Manley NR, Capecchi MR. Hox group 3 paralogous genes act synergistically in the formation of somitic and neural crest-derived structures. *Dev Biol*. 1997;192(2):274–288.
47. Jeannotte L, Lemieux M, Charron J, Poirier F, Robertson EJ. Specification of axial identity in the mouse: role of the Hoxa-5 (Hox1.3) gene. *Genes Dev*. 1993;7(11):2085–2096.
48. Watari N, Kameda Y, Takeichi M, Chisaka O. Hoxa3 regulates integration of glossopharyngeal nerve precursor cells. *Dev Biol*. 2001;240(1):15–31.
49. Maina F, Klein R. Hepatocyte growth factor, a versatile signal for developing neurons. *Nat Neurosci*. 1999;2(3):213–217.
50. Bartel FO, Higuchi T, Spyropoulos DD. Mouse models in the study of the Ets family of transcription factors. *Oncogene*. 2000;19(55):6443–6454.
51. Trimboli AJ, et al. Pten in stromal fibroblasts suppresses mammary epithelial tumours. *Nature*. 2009;461(7267):1084–1091.
52. Birchmeier C, Gherardi E. Developmental roles of HGF/SF and its receptor, the c-Met tyrosine kinase. *Trends Cell Biol*. 1998;8(10):404–410.
53. Watabe T, et al. The Ets-1 and Ets-2 transcription factors activate the promoters for invasion-associated urokinase and collagenase genes in response to epidermal growth factor. *Int J Cancer*. 1998; 77(1):128–137.
54. Chen Z, Fisher RJ, Riggs CW, Rhim JS, Lautenberger JA. Inhibition of vascular endothelial growth factor-induced endothelial cell migration by ETS1 antisense oligonucleotides. *Cancer Res*. 1997; 57(10):2013–2019.
55. Kitange G, et al. Ets-1 transcription factor-mediated urokinase-type plasminogen activator expression and invasion in glioma cells stimulated by serum and basic fibroblast growth factors. *Lab Invest*. 1999; 79(4):407–416.
56. Grider MH, Chen Q, Shine HD. Semi-automated quantification of axonal densities in labeled CNS tissue. *J Neurosci Methods*. 2006;155(2):172–179.